applied sciences

MDPI

Article

Impact of Various High Intensity Earthquake Characteristics on the Inelastic Seismic Response of Irregular Medium-Rise Buildings

Filip Pachla [1,*], Tadeusz Tatara [1] and Waseem Aldabbik [2]

[1] Faculty of Civil Engineering, Cracow University of Technology, 31-155 Cracow, Poland; tadeusz.tatara@pk.edu.pl
[2] Doctoral School, Cracow University of Technology, 31-155 Cracow, Poland; waseem.aldabbik@doktorant.pk.edu.pl
* Correspondence: filip.pachla@pk.edu.pl

Abstract: In the twenty-first century, the seismic design of buildings seems to have become a fully recognized topic. There are guidelines and standards which should be taken into account by designers in seismic areas. Designers using modern international guidelines have ascertained that the behavior of structures is not as expected. New challenges in the construction industry result in the construction of structures with new, unusual shapes. These are structures that do not meet the assumptions of safe construction in seismic areas. Contemporary buildings are also characterized by their irregular distribution of structural elements. Such solutions are not beneficial from the point of view of seismic engineering and can lead to reduced dynamic resistance and damage in such structures. In this paper, a five-storey, irregular-shaped reinforced concrete (RC) building model was subjected to different earthquakes with varying magnitudes, PGA (peak ground acceleration) and PGV (peak ground velocity) values, and durations of the intense shock phase. Once the model was verified using previous in situ measurements, the building model was subjected to five earthquakes. A numerical nonlinear analysis of the building was performed using a verified FEA (finite element analysis) model in the time domain through non-linear time history analysis with the Broyden–Fletcher–Goldfarb–Shanno (BFGS) method. The building's dynamic properties were measured using various methods of excitation. The model was influenced, among others, by two far-field representative events caused by the last earthquake in Turkey, which resulted in strong ground motion. The analysis results identified the locations of structural damage and allowed for the assessment of the structure's dynamic resistance. The results of the calculations prove that the duration of the intensive phase of extortion is one of the reasons for building damage in earthquake-prone areas. Building damage occurs with earthquakes that are characterized by an intensive phase of excitation with a long duration and high values of velocity in the earthquake components. The article highlights the inadequate dynamic resistance of the building, leading to excessive displacements and unfavorable structural solutions. Damage to buildings at this earthquake intensity caused damage to the load-bearing structure, which was not designed for such intensities. This paper is a research report with a specific case study of medium-rise irregular RC buildings.

Keywords: RC irregular structure; dynamic model; earthquake; time history analysis; dynamic response; damage

check for updates

Citation: Pachla, F.; Tatara, T.; Aldabbik, W. Impact of Various High Intensity Earthquake Characteristics on the Inelastic Seismic Response of Irregular Medium-Rise Buildings. *Appl. Sci.* **2024**, *14*, 9740. https://doi.org/10.3390/app14219740

Academic Editor: Dario De Domenico

Received: 16 September 2024
Revised: 22 October 2024
Accepted: 23 October 2024
Published: 24 October 2024

Copyright: © 2024 by the authors. Licensee MDPI, Basel, Switzerland. This article is an open access article distributed under the terms and conditions of the Creative Commons Attribution (CC BY) license (https://creativecommons.org/licenses/by/4.0/).

1. Introduction

Earthquakes, a natural phenomenon, have shaped our planet since the beginning. Their intensity varies, ranging from barely noticeable tremors to catastrophic seismic events that can alter the course of civilizations and reshape cities. The destructive power of earthquakes is immense, often resulting in a significant loss of life and widespread

devastation. Moreover, they can set off tsunamis, as witnessed during the 2004 Indian Ocean earthquake, further amplifying their destructive potential. These seismic events, while devastating, are an integral part of Earth's dynamic nature [1].

1.1. Review of Chosen Former Intense Earthquakes

Between 1998 and 2017, earthquakes caused about 750,000 deaths globally, accounting for over half of all fatalities from natural disasters (https://www.who.int/health-topics/earthquakes#tab=tab_1, accessed on 19 August 2024). During this period, earthquakes affected over 125 million people, leading to injuries, homelessness, displacement, or evacuation during the emergency phase (https://www.who.int/health-topics/earthquakes#tab=tab_1, accessed on 19 August 2024). A study by [2] provides valuable information concerning the intensity of earthquakes and the damage observed in Greece and its surroundings from 550 B.C. to 1975. Historically, numerous massive earthquakes have resulted in significant death tolls and extensive damage to infrastructure. For instance, the eruption of the volcano Vesuvius in 79 AD led to the infamous Pompeii earthquake, causing up to 16,000 deaths and completely covering the city of Pompeii in ash and lava [3]. In 1700, the west coast of the United States experienced a catastrophic earthquake with an estimated magnitude of 8.7–9.2 [4]. Between 1811 and 1812, the New Madrid Seismic Zone in the central United States was hit by a series of powerful earthquakes, with magnitudes ranging from 7.2 to 8.2, causing widespread damage and altering the course of the Mississippi River [5]. In 1755, a 9.0 magnitude earthquake devastated Lisbon, resulting in an estimated death toll of 60,000 to 100,000 people in Portugal, Spain, and Morocco due to the earthquake, subsequent fires, and a tsunami [6]. The San Francisco Earthquake of 1906, one of the largest earthquakes in the United States, with a magnitude of 7.9, caused extensive destruction in San Francisco and resulted in an estimated death toll of approximately 3000 people [7]. The 1960 earthquake, also known as the Great Chilean earthquake, is the most powerful earthquake ever recorded worldwide. It occurred in the Valdivia region of Chile and is estimated to have measured between 9.4 and 9.6 on the Richter scale. The earthquake resulted in around 1600 deaths, thousands of injuries, and widespread damage to infrastructure, industries, and agriculture [8]. The Great Alaska Earthquake of 1964, with a magnitude of 9.2, caused extensive damage to Southcentral Alaska and triggered a massive tsunami, remaining the most powerful earthquake ever recorded in North America [9]. The Kobe earthquake in 1995, with a magnitude of 7.2, caused significant damage in Kobe, Japan, resulting in over 5500 deaths, more than 41,000 injuries, and the destruction of over 100,000 homes [10]. In 2011, Japan was struck by a massive 9.0 magnitude earthquake, leading to a triple disaster involving an earthquake, tsunami, and nuclear accident, resulting in approximately 20,000 deaths and injuries to more than 6000 people. Over 470,000 people were evacuated from their homes [11]. The disaster also triggered a severe accident at the Fukushima nuclear power plant, considered one of the worst nuclear incidents in history [12]. The earthquake resulted in financial losses of approximately USD 200 billion, making it the costliest in history. In 2015, a devastating 7.8 magnitude earthquake hit Gorkha, Nepal, claiming more than 9000 lives, injuring over 23,000 people, and displacing millions. The earthquake triggered avalanches and landslides and destroyed around 500,000 buildings [13]. The 2023 Gaziantep earthquake in Turkey, with a magnitude of 7.8, is the most severe natural disaster ever recorded in the history of both Turkey and Syria. The earthquake resulted in an estimated 50,000 fatalities in both countries. As of mid-February 2023, more than 25,000 buildings were destroyed in Turkey, and the condition of 170,000 structures must be examined [14].

1.2. Metodologhy of Seismic Analysis

The seismic analysis of structures involves both linear and nonlinear methods, and these have been incorporated into the latest European and US seismic design codes. Some of these methods include non-linear dynamic time-history analysis, the N2 non-linear static method (Eurocode 8 [15]), the non-linear static procedure NSP (FEMA 356 [16]), and the improved capacity spectrum method CSM (FEMA 440 [17]). FEMA Report 356 [16] presents performance-based engineering methods that rely on nonlinear static analysis procedures to predict structural demands. This procedure involves generating a "pushover" curve to predict the inelastic force–deformation behavior of the structure, which is used to calculate the inelastic displacement demand for a given ground motion. The report also uses the Coefficient Method to calculate the displacement demand by modifying elastic predictions of the displacement demand.

The primary goal of the report [17] is to evaluate and improve the nonlinear static procedures (NSPs) contained in FEMA 356 [16] and the Applied Technology Council ATC-40 report [18]. It also aims to provide a guide concerning when and how each methodology should be used to avoid conflicting answers. Among these methods, the N2 method [19] is widely used in structural engineering for seismic design and assessment. It is outlined in Eurocode 8 [15] and is commonly employed for performance-based seismic design. The key advantage of the N2 method lies in its use of the relationship between the base shear force and the roof displacement of a structure during an earthquake to create a capacity curve. This curve is simplified into two linear segments: an initial elastic segment and a subsequent plastic segment, transforming it into an equivalent Single-Degree-of-Freedom (SDOF) system. In the N2 method, the target displacement, representing the expected maximum displacement during an earthquake, is determined using the response spectrum of the equivalent SDOF system. Finally, this target displacement is compared to the capacity curve to evaluate the performance of the structure and assess whether it can withstand expected seismic forces without significant damage. All numerical models are typically expected to have a degree of uncertainty [20,21].

Modern construction presents challenges for builders today, not only in constructing bridges with varied structures but also in building tall and very tall buildings. Buildings can have irregular shapes due to architectural vision, seen through architectural design, structural elements, and various forms of irregularity. These irregularities could include asymmetrical facades, structural irregularities, irregular floor plans, irregular building shapes and materials, irregular historical buildings, the adaptive reuse of irregular buildings, irregular building codes or zoning regulations, natural irregularities, building maintenance irregularities, and buildings with irregular heights or setbacks. Addressing these irregularities often requires interdisciplinary collaboration among architects, engineers, contractors, and regulatory agencies. Despite the challenges they may pose, irregularities in buildings contribute to the diversity and character of architectural landscapes, reflecting the creativity and adaptability of human design. Earthquakes are dangerous and destructive natural events that can cause significant material and human losses, especially for these types of irregular structures. However, advances in science and technology are contributing to predicting and minimizing their impact, and protecting societies from harm. It is essential to design and construct structures that can withstand earthquakes, and new technologies and regulations such as Eurocode 8 [15] can help achieve this goal. Besides earthquakes, similar phenomena caused by factors such as traffic and mineral resource extraction, like coal and copper ore, can also cause tremors.

This article presents numerical studies conducted on five different types of excitation for five-story irregularly shaped RC building models made of two different materials: reinforced concrete (RC) and masonry. The excitations were assumed to be surface horizontal vibrations from earthquakes, with five representative far-field events, including the latest earthquake in Turkey, influencing the models. Velocity refers to the amount of energy transferred to the object and influencing the damage state [22]. The objective is to

compare the results of numerical analyses of structures made from two different materials under the same soil conditions, focusing on the duration of earthquake excitations and their impact on structural responses. The study details the numerical analyses of the nonlinear finite element method (FEM) model of the experimentally verified RC building with irregularities, which was previously studied in [23]. The study used time history non-linear analysis with nonlinear concrete and masonry models. The results allow for the assessment of the seismic behavior of the structure, the estimation of the influence of earthquake parameters on the dynamic response, and the identification of structural damages and dynamic resistance.

This paper fills the gap in the literature concerning the influence of earthquakes on irregular structures. In recent years, the issue of the impact of earthquakes on irregular structures has been the subject of regular conferences with the participation of specialists in this field [24–27]. Recent studies on the effect of various earthquake parameters on the behavior of structures are included in, e.g., [28,29], while the effects of earthquakes on structures can be found in, e.g., [30,31].

2. Ground Motion Parameters

To understand how structures respond to dynamic loading such as earthquakes, it is crucial to perform dynamic analysis. A comprehensive documentation of the horizontal components of ground acceleration is necessary to accurately evaluate the impact of vibrations on structures and determine the system's dynamic response. In this work, five representative seismic events were adopted. The events were selected based on the intensity described by PGA and PGV and the duration of the intense phase of duration. The authors also took into consideration the value of the PGA/PGV parameter. Historical tremors such as El Centro and current ones concerning earthquakes in Turkey in 2023 were selected.

A summary of the characteristics of the five earthquakes that were selected for analysis is provided in Table 1.

Table 1. Characteristics of the analyzed components of vibrations.

Parameter	Direction	Station No. 2703	Station No. 3134	Sitka	El Centro	L'Aquila
Magnitude [-]		7.8	7.8	7.3–8.1	6.9	6.3
PGA (mm/s^2)	X	1650.64	2039.09	765	2099.3	2677
	Y	1566.34	2461.07	894	3423	3975
PGV (mm/s)	X	165.29	396.42	74.2	487.9	109
	Y	130.67	391.53	67	380.9	318
PGA/PGV (s^{-1})	X	9.986	5.144	10.3	4.3	24.5
	Y	11.987	6.286	13.3	9.0	12.5
t * (s)	X	52.68	44.56	28.88	24.42	7.4
	Y	52.16	44.83	27.1	24.54	8.1

* Duration of the intensive phase of acceleration.

The waveform of the horizontal components of the vibration accelerations from the districts of stations No. 2703 and No. 3134 for the Turkey–Syria, Sitka, L'Aquila, and El Centro earthquakes, along with Husid's graphs and the results of the FFT analysis of the records, are displayed in Figures 1–5. The Husid plot was used to calculate the strong motion duration for the horizontal components [22,32].

The vibration records from Figures 1 and 2 reveal that the primary frequencies of the ground acceleration vibrations are consistently below 5Hz. Furthermore, the maximum values of the horizontal components x and y (PGAx, PGAy) of the acceleration records in station No. 3134 were found to be higher than the corresponding components of the vibrations in station No. 2703—comp. This is shown in Figures 1 and 2, and Table 1. Station No. 2703 and 3134 are located on grounds A and B corresponding to Eurocode 8 [15], respectively.

In summary, these earthquakes were incredibly destructive, resulting in a significant loss of life and property damage. The seismic activity also had a significant impact on the region's infrastructure, as many buildings were destroyed or damaged.

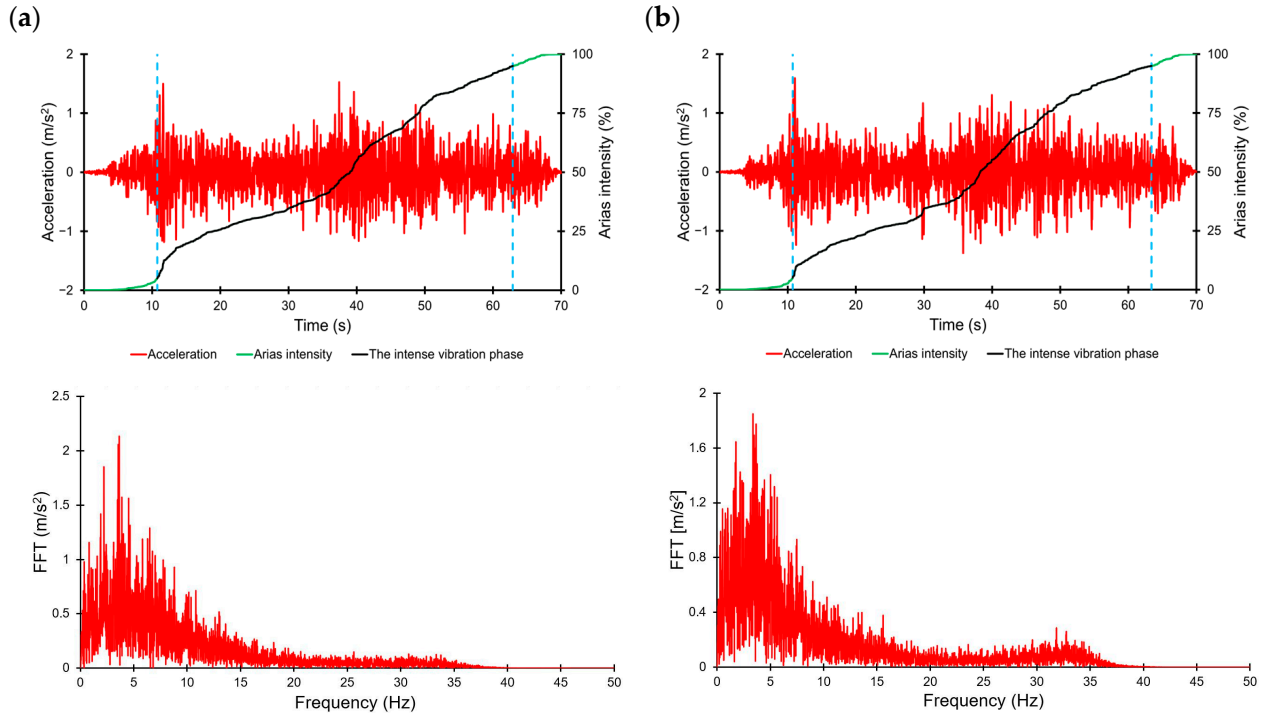


Figure 1. Earthquake station No. 2703: (**a**) EW direction; (**b**) NS direction.

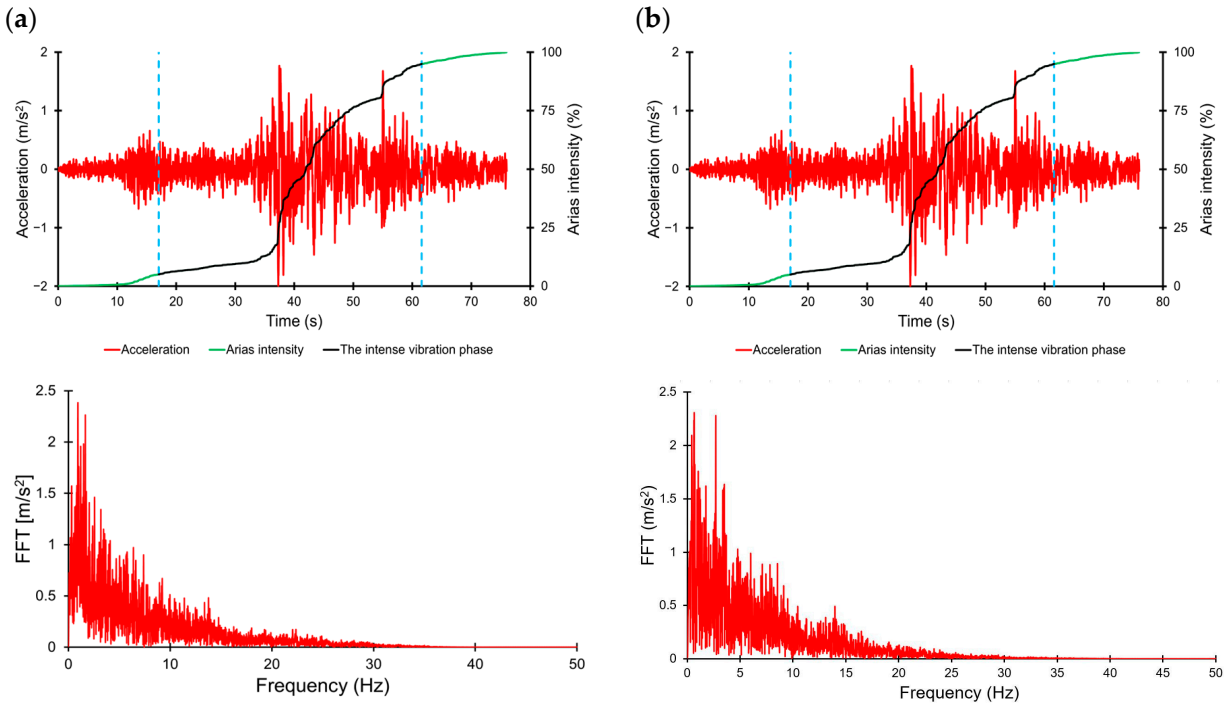


Figure 2. Earthquake station No. 3134: (**a**) EW direction; (**b**) NS direction.

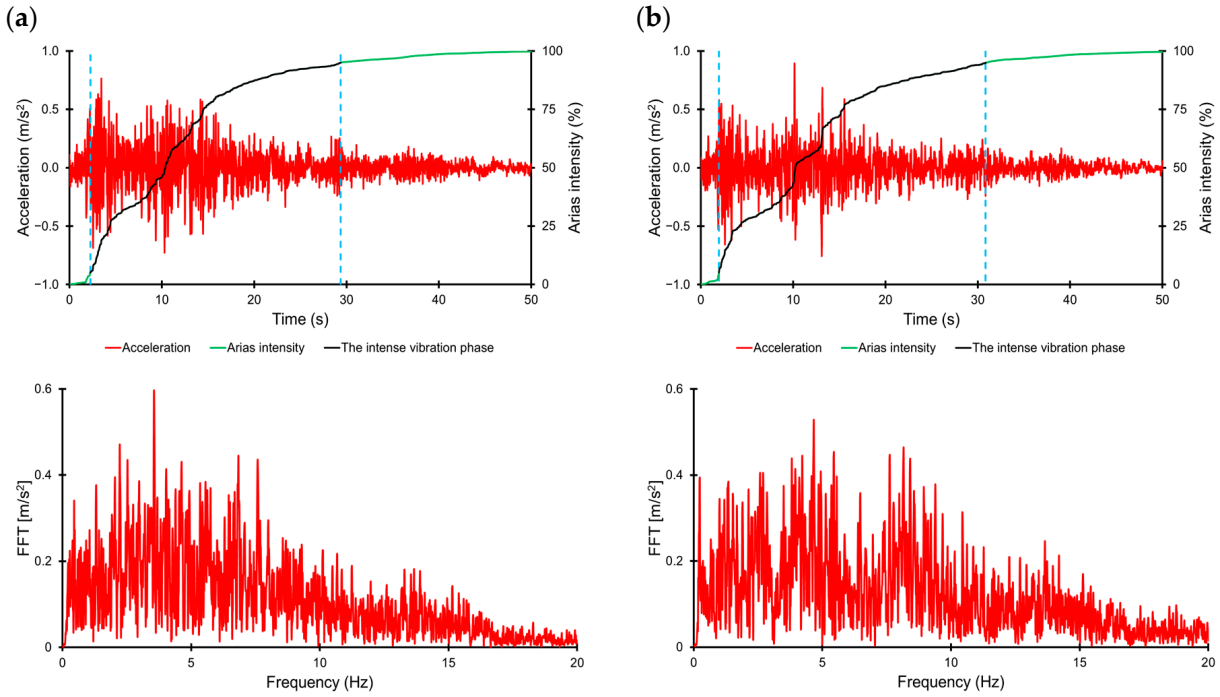


Figure 3. Components of x (**a**) and y (**b**) for Sitka earthquake.

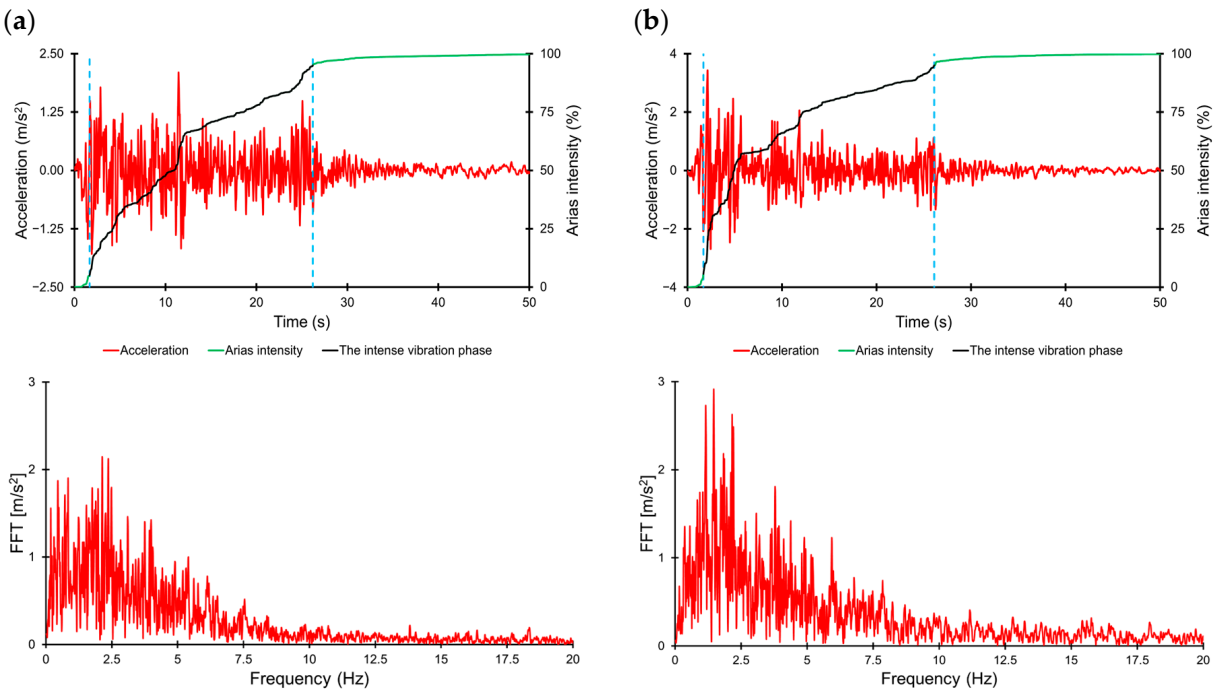


Figure 4. Components of x (**a**) and y (**b**) for the El Centro earthquake.

On 30 July 1972, an earthquake occurred 48 km away from Sitka, Alaska, in the US. The earthquake had a magnitude of Mw between 7.3 and 8.1 [33]. Fortunately, there were no reported injuries or loss of life, and only minor damage was reported. However, light damage was observed in Hoonah, Juneau, Pelican, and Yakutat [34,35]. The cause of the earthquake was linked to the existence of the Fairweather–Queen Charlotte fault, which resulted in several intense shakes from 1949 to 1972 [36,37]. An example of the horizontal acceleration vibrations recorded in the x and y components is presented in Figure 3.

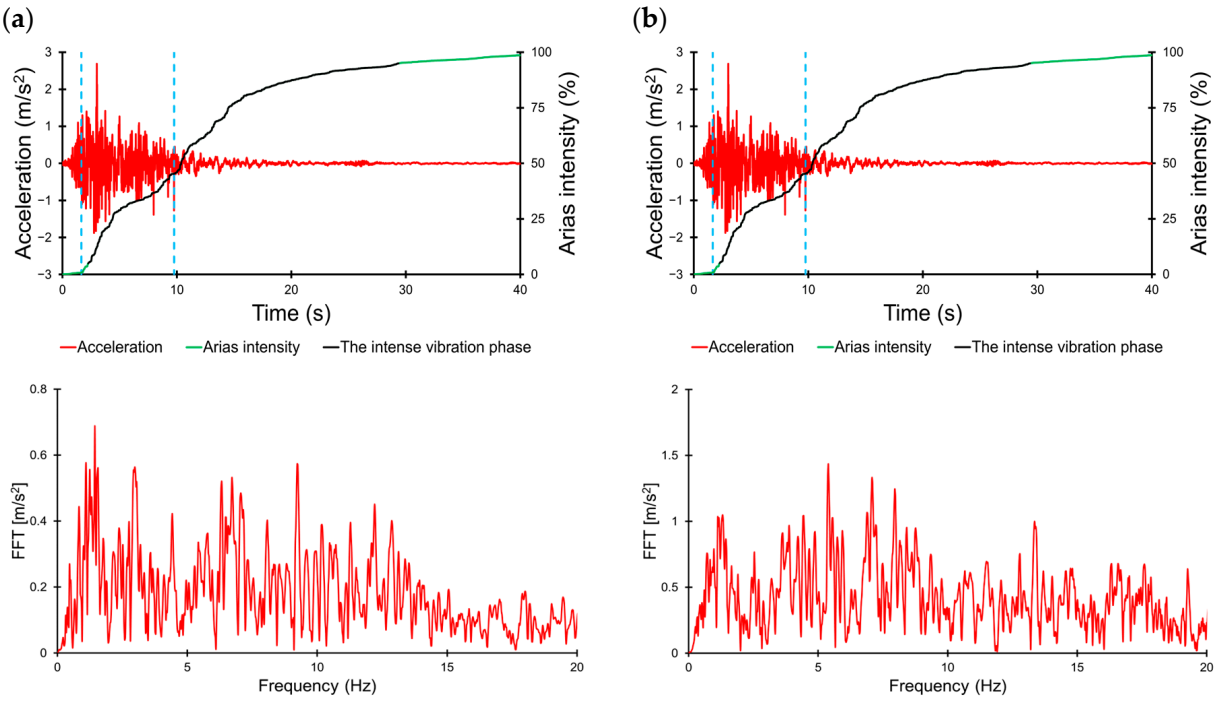


Figure 5. Component of x (**a**) and y (**b**) for L'Aquila earthquake.

In 1940, a powerful earthquake struck the Imperial Valley in California, known as the El Centro earthquake. The earthquake had a magnitude of 6.9 and resulted in a maximum displacement of 4.5 m [38,39]. According to the authors of [39], an event is defined as an occurrence of energy release that generates seismic phases, which can be resolved and identified. They stated that the size of those discrete events was abnormally strong compared to regular aftershocks. The earthquake caused extensive damage to irrigation systems and resulted in the death of nine people. The horizontal components of the acceleration vibrations are displayed in Figure 4.

The earthquake that occurred on 6 April 2009, in the city of L'Aquila (Italy) and the surrounding areas, was the most recently analysed [40,41]. It had a magnitude of 6.3 on the Richter scale and had devastating consequences for the inhabitants. A total of 309 people lost their lives, around 1500 were injured, and approximately 40,000 people lost their homes. Additionally, it caused damage to around 18,000 buildings in the epicenter area. The horizontal components of the L'Aquila earthquake are depicted in Figure 5.

The earthquakes that were analyzed had a high magnitude, ranging from 6.3 to 8.1. The values of PGA and PGV were also among the highest recorded for earthquakes. The PGA component ranged from 765 to 3973 mm/s^2, while the PGV component ranged from 67 to 487.9 mm/s. The ratio of PGA/PGV for these earthquakes falls within the typical range of 4.3 to 24.5 s^{-1}. The "strong phase" duration for both horizontal components x and y were practically the same, ranging from 7.4 to 53 s, as shown in Table 1.

3. Nonlinear Dynamic Analysis

The surface vibrations detected during the earthquakes were examined as part of our research on the impact of earthquakes on buildings. A dynamic analysis of an irregular building was performed, using the horizontal components of five earthquakes accompanied by near-source ground-bore motion, to gain a better understanding of this. It is important to note that two phenomena unique to the Turkey and Syria earthquakes, which were of comparable intensity and recorded at seismic stations located on two different site classifications (A and B), as defined by EC-8 [15], were investigated in the paper. The dynamic behavior of the structure was studied using a non-linear time history analysis (THA), where earthquake records were used as kinematic loading. The analyses were conducted in two stages, explained in detail

in reference [23]. The Finite Element Diana code [42] was used for the calculations, and the Broyden–Fletcher–Goldfarb–Shanno (BFGS) method [43–47] was used for solving non-linear problems, performing the time history analysis (THA), and observing the development of cracks. This method belongs to the class of quasi-Newton methods. The stiffness of the model was updated with a constant time step, meeting the convergence criterion based on the relative norm of the last displacement increment vector [42]. The material characteristics and parameters are detailed and listed in [23].

3.1. FEA Model

For the analysis, a five-story building with an irregular structure was chosen. It was constructed using reinforced concrete walls and columns, along with masonry infill walls. The building measures 17.6 m by 17.9 m and stands at a height of 23.2 m. The concrete staircases are located on the northern side of the building. The columns have different cross-sections, ranging from 25 cm by 25 cm to 35 cm by 35 cm, and the ceiling slabs are 25 cm thick. For further details, please refer to Figure 6, which includes the 4th floor plan, cross-section, and the FEM model of the building.

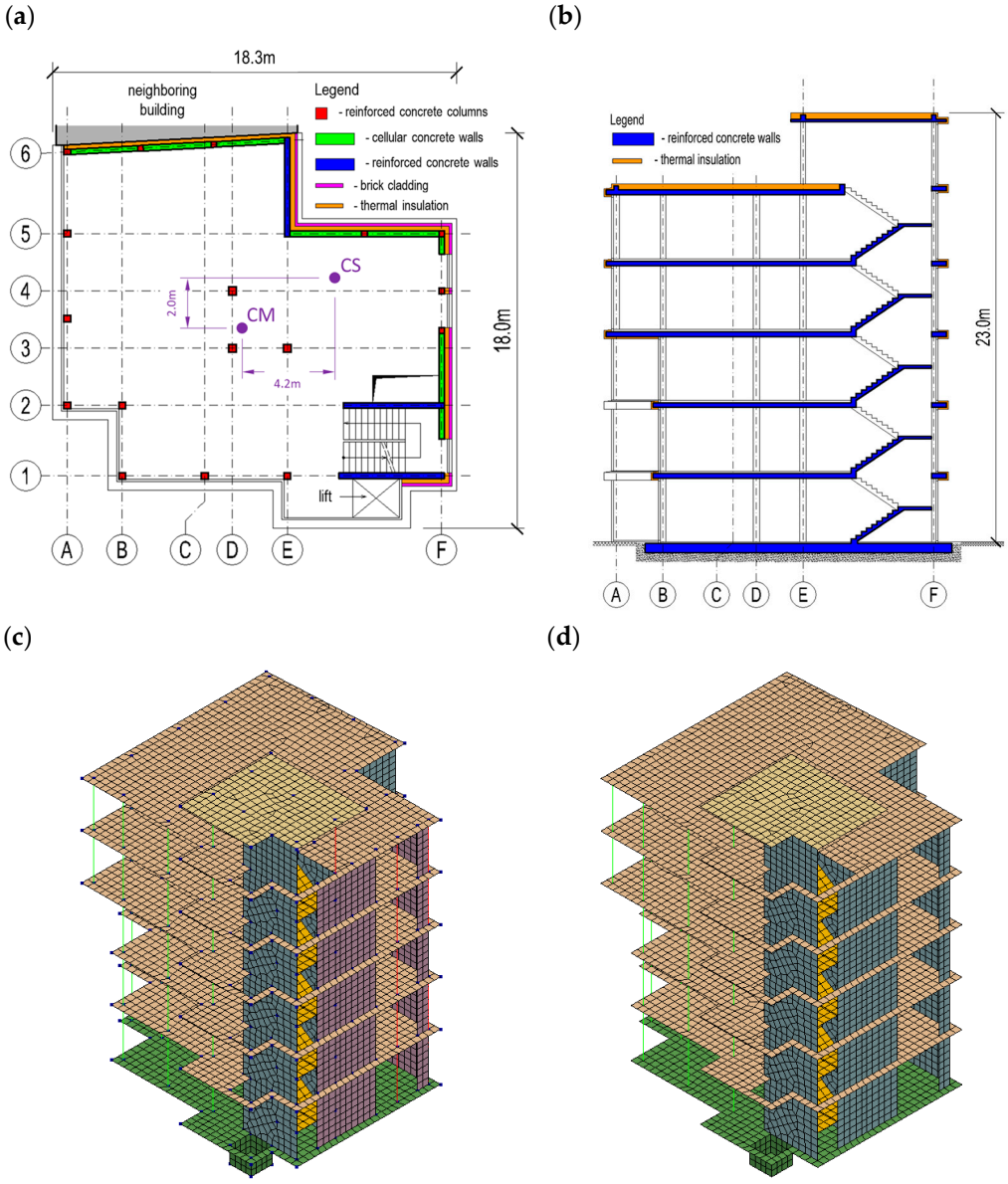


Figure 6. View of the building: (**a**) plan of the 4th floor; (**b**) cross-section of the building; (**c**) FEM model No. 1—masonry and RC walls [23]; (**d**) FEM model No. 2—RC walls.

The building was previously studied in [23]. The model of the selected building with irregularities was experimentally verified in [23]. The dynamic properties were measured using different excitation methods [23].

This study details the numerical study of the nonlinear FEM model. The first variant of the model (model No. 1) corresponds to cellular masonry and RC-bearing walls. The second variant of the model (model No. 2) consists only of the RC-bearing walls. The first material creating the bearing walls of the building corresponds to the actual structure. The locations of the center of mass (CM) and the center of stiffness (CS) are shown in Figure 6.

The FEM was applied to create a spatial model for the dynamic analysis of a building. The model involves all significant elements that affect the stiffness and mass distribution and determines the building's dynamic properties. Due to the irregularity of the load-bearing element positions, the construction of the model could not be simplified. The foundation level of the model is supported by fixed translation and rotational degrees of freedom. The structural model assumed for further analysis is presented in Figure 6. It is worth noting that the last floor of the building does not cover the entire roof area, as shown in Figure 6c,d. A detailed description of the model and dynamic in situ research on the building were presented in paper [23]. Dynamic in situ tests were conducted using several building excitations, including a modal hammer, traffic on a nearby street, and controlled rides of a light truck through the threshold release [23]. The measured and calculated eigenfrequencies are listed in Table 2 and presented in Figure 7.

Table 2. Natural frequencies of the model based on dynamic measurements.

Mode Shape	Measured Values of Frequency [Hz]	Calculated Values of Frequency [Hz]
Flexural in 'y' direction	1.89	1.84
Flexural in 'x' direction	2.62	2.65
Torsional	(2.5–3.5)	3.35

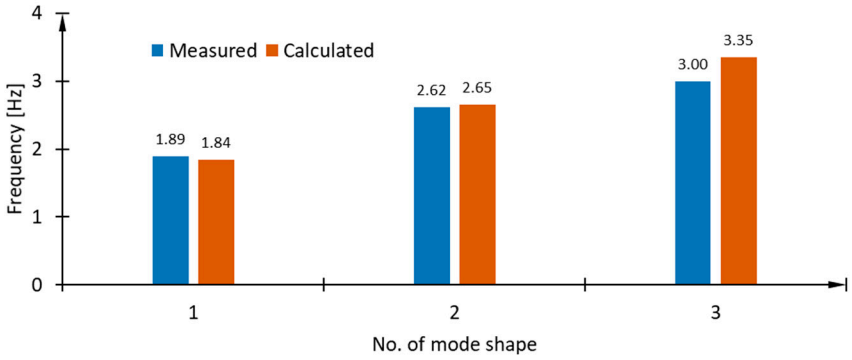


Figure 7. Histogram of measured and calculated natural frequencies of the building.

3.2. Results of the Dynamic Response and Discussion

Exemplary maximum horizontal forces (base shear) calculated using the THA method for the analysis model after a nonlinear analysis are shown in Figures 8 and 9 for Model No. 1 and Figures 10 and 11 for Model No. 2, calculated using the most intense earthquake. The calculated resultant displacements due to excitation from station No. 3134 are observed to be higher than those for the load from station No. 2703 in model No. 1 and model No. 2. This difference is because the values of PGA and PGV obtained from the records at station No. 3134 are higher than the values obtained at station No. 2703 (comp. Figures 1 and 2 and Table 3). A comparison of the obtained base shear values in the analyzed models for all excitations is presented in Figure 12.

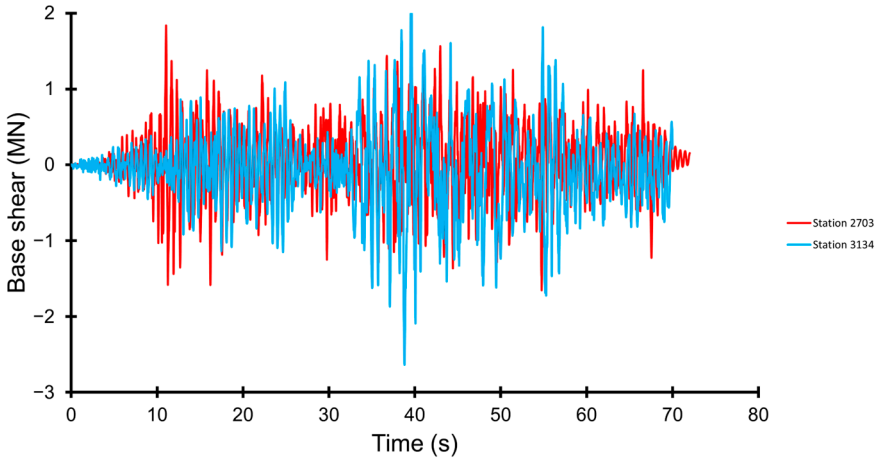


Figure 8. Maximum horizontal force (Base Shear) for stations No. 2703 and No. 3134 for model No. 1—masonry and RC walls.

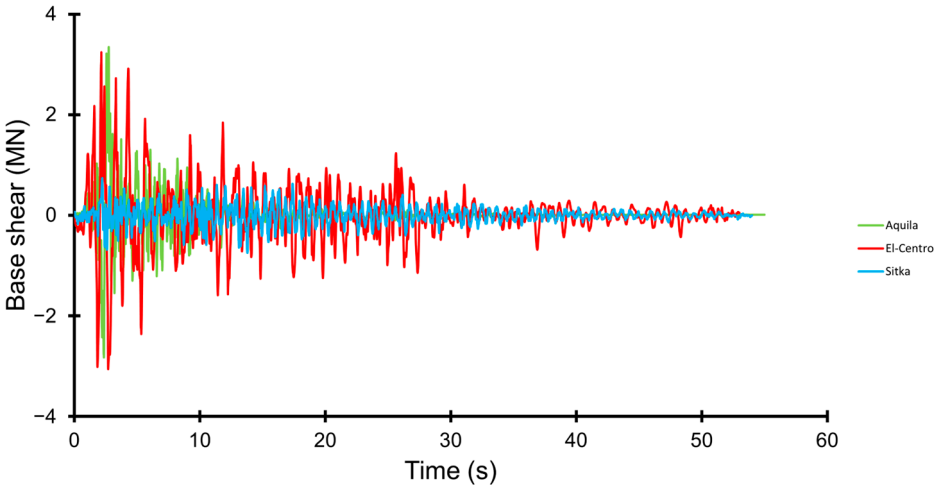


Figure 9. Maximum horizontal force (Base Shear) for Aquila, El-Centro, and Sitka for model No. 1—masonry and RC walls.

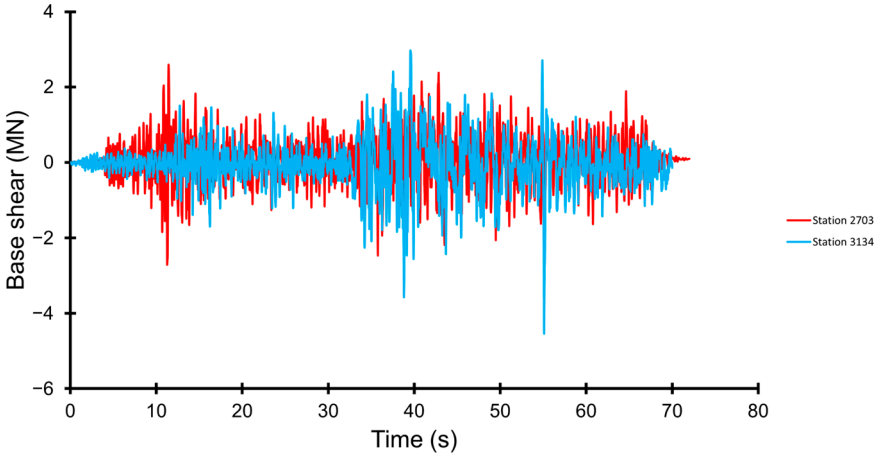


Figure 10. Maximum horizontal force (Base Shear) for stations No. 2703 and No. 3134 for model No. 2—RC walls.

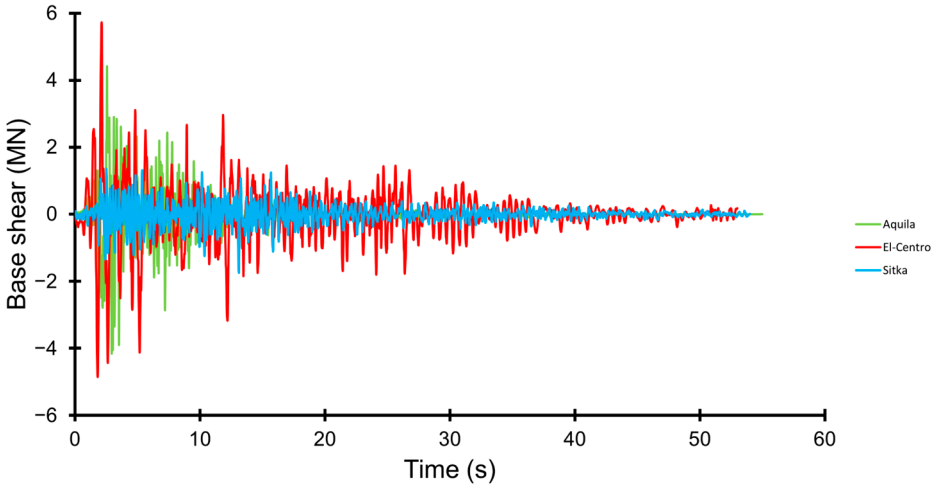


Figure 11. Maximum horizontal force (Base Shear) for Aquila, El-Centro, and Sitka for model No. 2–RC walls.

Table 3. Calculated base shear force.

Selected Results	Excitations from the Station				
	Station No. 2703	Station No. 3131	Sitka	El Centro	L'Aquila
No.	1	2	3	4	5
Base Shear, MN for model No. 1	1.84	2.88	0.65	3.31	3.35
Base Shear, MN for model No. 2	2.60	2.98	1.25	5.81	4.42

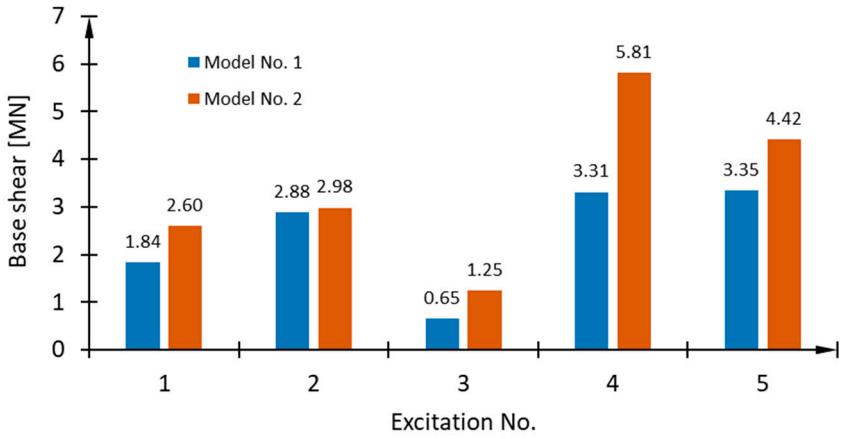


Figure 12. Histogram of calculated base shear force.

The results from Table 3 indicate that the highest base shear force can be observed in the L'Aquila earthquake and El Centro earthquake in model No. 1 and model No. 2, respectively. Despite the significantly shorter duration time of the intense phase for the L'Aquila earthquake, the base shear force is highest in model No. 1. The base shear force from event 3134 is higher than that from event 2703; the reason for this is that the horizontal vibration components had significantly higher PGA and PGV values. The results from Table 3 also indicate that the base shear force from Model No. 2 is higher than that of Model No. 1 (comp. Figure 12).

The exemplary resultant maximum horizontal displacement for the analysis model using the THA method after a nonlinear analysis is shown in Figures 13 and 14. The calculated values of the resultant displacements from the excitation from station No. 3134

(Figure 13b) were found to be higher than those from station No. 2703 (Figure 13a). The reason for this is that the horizontal vibration components had significantly higher PGA and PGV values.

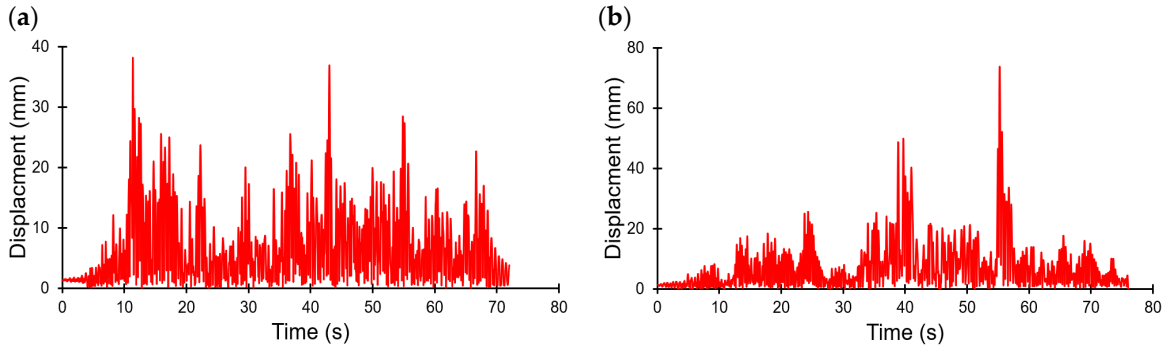


Figure 13. Calculated resultant displacements for excitation from station: (**a**) No. 2703; (**b**) No. 3134 for model No. 1—masonry and RC walls.

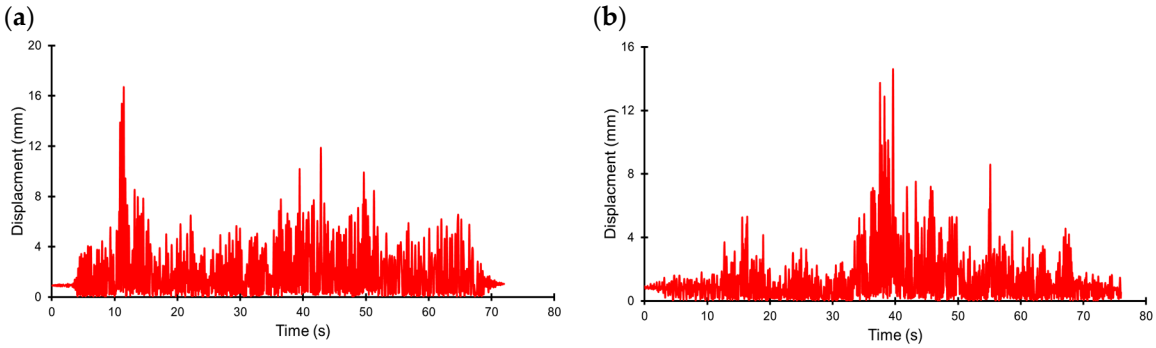


Figure 14. Calculated resultant displacements for excitation from station: (**a**) No. 2703 and (**b**) No. 3134 for model No. 2—RC walls.

The values of the resultant displacements were calculated using the following formula:

$$D = \sqrt{X^2 + Y^2} \quad (1)$$

The calculated values for the analyzed earthquakes are shown in Table 4.

Table 4. The resultant displacements in the X-Y directions for the whole building, mm.

Selected Results	Excitations from the Station				
	Station No. 2703	Station No. 3134	Sitka	El Centro	L'Aquila
Maximum relative displacement between the roof and 6th floor in Model No. 1	20.22	32.00	20.67	57.60	21.49
Maximum relative displacement between 6th floor and foundation in Model No. 1	16.68	31.74	8.26	60.02	36.72
Resultant maximum displacement in Model No. 1	26.15	54.03	26.40	96.14	49.52
Maximum relative displacement between roof and 6th floor in Model No. 2	33.26	42.62	23.85	62.41	27.67
Maximum relative displacement between 6th floor and foundation in Model No. 2	15.91	24.44	7.55	58.38	18.59
Resultant maximum displacement in Model No. 2	33.33	44.38	23.06	62.41	28.04

The results from Table 4 indicate a significant displacement between the highest part of the building's roof and the level of the 6th floor ceiling. This disparity is due to the roof's role as a support. However, such variations should not be allowed under seismic loads. The displacement between the ceiling of the 6th floor and the foundation is smaller, due to the presence of a stiffening wall that spans the height of the building.

The results from Table 4 show that the displacement from event 3134 is higher than that from event 2703. The displacements in Model No. 1 are higher than those in Model No. 2 for all earthquake vibrations, except for the max displacements between the roof and the level of the 6th floor ceiling. The inter-story drift the in X and Y directions is presented in Figures 15 and 16. From the comparison of Figures 15 and 16, it can be seen that in the Y direction, the inter-story drift is larger than in the X direction due to a higher stiffness in the X direction. The inter-story drift values for the El Centro earthquake are the largest.

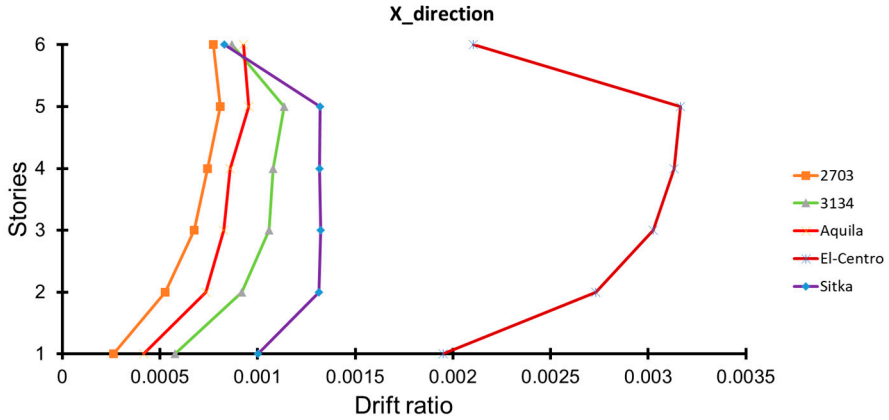


Figure 15. Inter-story drift in X direction for model No. 1.

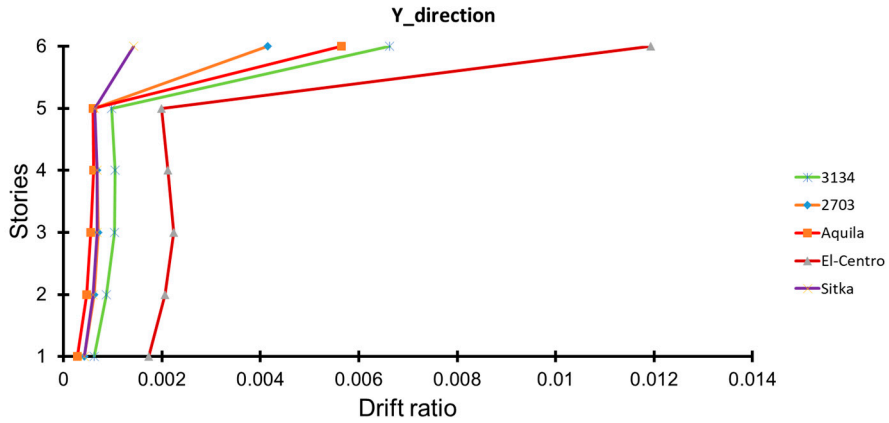


Figure 16. Inter-story drift in Y direction for model No. 1.

The localization of the crack patterns during specific earthquakes and the development of a crack pattern in the model are presented in Figures 17–20. The northeast part of the building had the most cracks, caused by the concentration of structural elements in this corner (staircase and elevator shaft) and the seismic loads absorbed by these elements. Based on the analysis, an asymmetrical arrangement of structural elements is not beneficial because of the dynamic resistance. It is important to note that the velocity of the horizontal components of ground vibrations has a significant impact on the building model's dynamic response. Analyzing Figures 17–20, a characteristic mechanism of destruction can be seen in the column elements at the connection with the ceiling shield. Cracks are concentrated there, indicating the plastic deformations of the elements in the range of tensile stresses. The degree of changes in this damage can be observed during the shock, as shown in Figures 17–20. Additionally, in the stiffening shear-wall elements, cracks occur, mainly at the connection of the walls with the foundation slab and the ceiling slabs for the individual

stories. These indicate the plastic deformations of the structural elements at the story level. This is also confirmed by high inter-story drift values (see Figures 15 and 16).

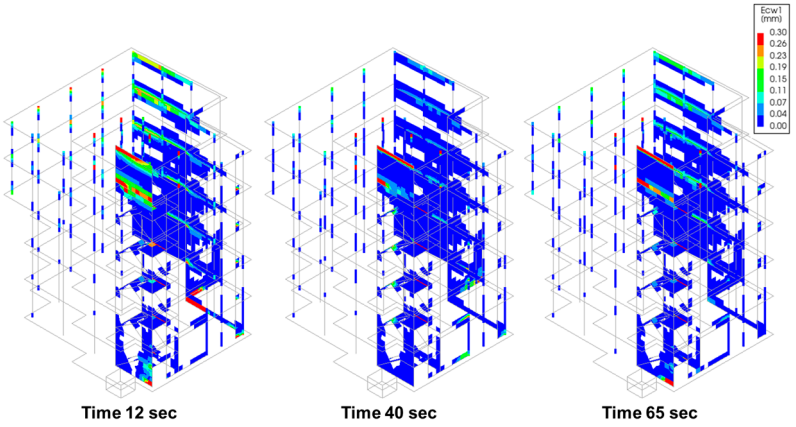


Figure 17. Crack width for Turkey earthquake record—station No. 2703 for Model No. 1—masonry and RC walls.

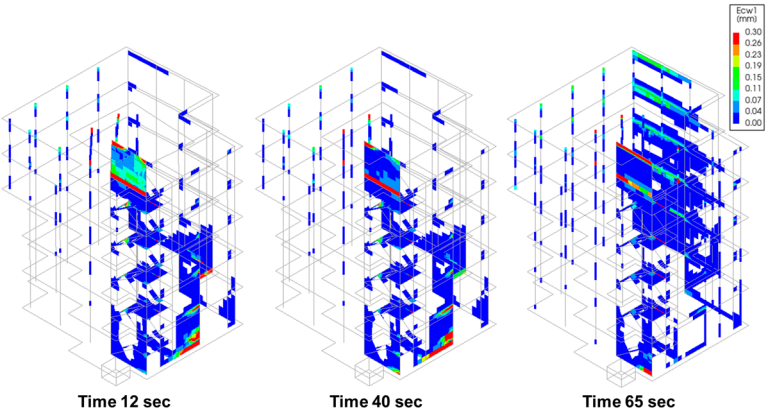


Figure 18. Crack width for Turkey earthquake record—station No. 2703 for Model No. 2—RC walls.

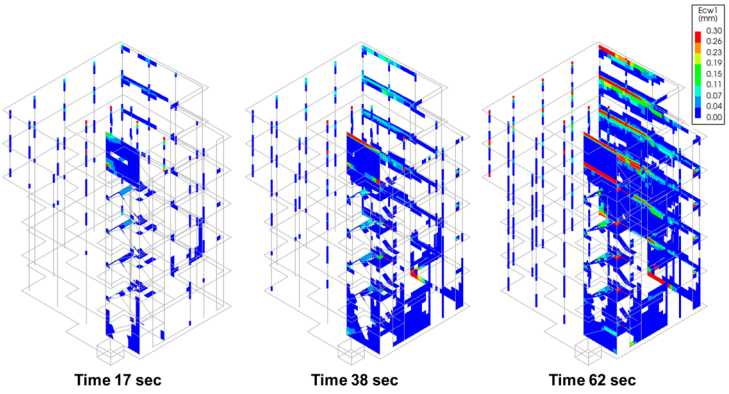


Figure 19. Crack width for Turkey earthquake record—station No.3134 for Model No. 1—masonry and RC walls.

A summary of the damage to structural elements (shear walls and columns) caused by the earthquakes analyzed using the building model is presented in Table 5. The Sitka earthquake caused cracks in the structural elements while other earthquakes resulted in structural damage. The damage in the form of cracks causes a degradation in the stiffness of the entire model. As a result, the object is less resistant to further aftershocks. Some of the cracks may be closed, but the stiffness of the element in this area remains weakened. The literature provides solutions that prevent the degradation of structural

systems, such as hybrid braced frames (HBFs) and self-centering viscous energy-dissipative braces (SCVDBs) [48,49]. Due to the fact that the analyzed building did not have such elements, they were not included in this work.

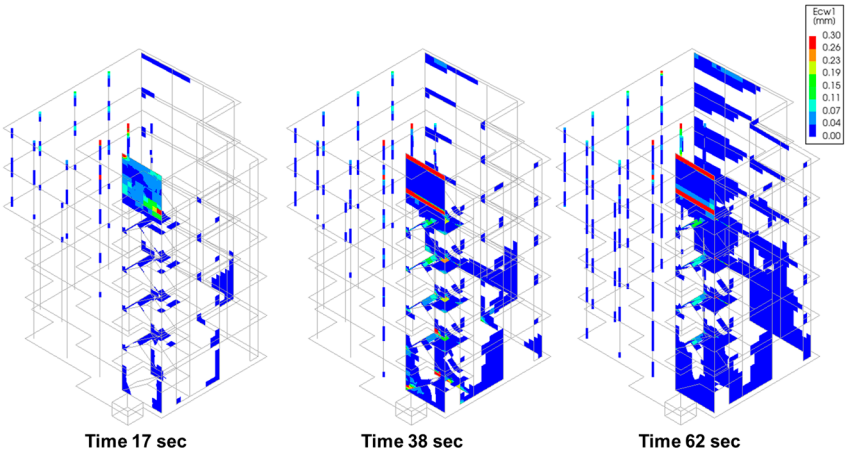


Figure 20. Crack width for Turkey earthquake record—station No.3134 for Model No. 2—RC walls.

Table 5. Summary of damages.

Type of Excitation	Type of Damage	Degree of Damage
Turkey earthquake No. 2703—very high PGA values, long duration	Damages in structural elements	High
Turkey earthquake No. 3134—very high PGA values, long duration	Damages in structural elements	High
Sitka earthquake—small PGA values, long duration	Cracks in structural elements	Slight
El Centro earthquake—very high PGA values, long duration	Damages in structural elements	High
L'Aquila—very high PGA values, short duration	Damages in structural elements	Moderate

4. Conclusions

The article presents the findings of dynamic non-linear analyses performed for two irregular models of a building in response to five different types of earthquakes. The conclusions from the analysis are as follows:

- The first model consists of RC and masonry walls and the second model consists of just RC walls. The building's dynamic characteristics were examined before the calculations. The calculations focused on the base shear, displacement, and evaluation of the damage caused by the earthquakes.
- The study highlights that changes in seismic characteristics can significantly affect a building's dynamic response.
- The main contribution of this study is its attempt to consider the effect of different earthquakes with varying magnitudes, PGA and PGV values, and durations of the intense shock phase on the behavior of medium-rise structures. The level of ground velocity (PGV) has the most significant impact on structural damage. The horizontal velocity earthquakes analyzed ranged from 67 to 487.9 mm/s.
- The locations of structural damage were identified, and the dynamic resistance of the structure was assessed. It was observed that there is a significant displacement between the highest point of the building's roof and the level of the 6th floor ceiling. This displacement is caused by the design of that section of the building, which functions as a cantilever. However, the displacement between the ceiling on the top

floor and the foundation is smaller, due to the stiffer bearing wall throughout the height of the building. Based on these observations, it is recommended that such floors are not constructed in areas prone to earthquakes.

- The results of the calculations have led to significant conclusions. These findings should be taken into account when constructing new buildings or demolishing old ones. It is essential to avoid several design flaws, such as fragile columns, insufficient steel reinforcement, the improper tying of transverse reinforcement bars, the absence of beams and shear walls (even in tall buildings), improperly sized top floors, and incorrect joints.
- The presented analysis results are a supplement to research on the impact of seismic shocks on buildings with irregular structures. The results were presented for a specific building with a mixed irregular structure (column-wall) structure. The results obtained are consistent with the results obtained by other authors [20,24,25].

The limitations of this article result from the analysis being performed for a building of a specific irregularity for selected intense near-field earthquakes. Moreover, the article only refers to five selected seismic events; therefore, statistical studies were not conducted. Future analyses should be extended to include phenomena of lower intensity (far field). In the future, a larger number of seismic events should also be included in order to develop statistical relationships. It is worth noting that despite the significant earthquakes that occurred in Turkey in 2023, causing severe damage to over 130,000 buildings, the ones built by the Turkish Housing Development Administration (TOKI) in the earthquake-prone areas of ten provinces, centered in Kahramanmaras, remained structurally sound. The earthquake-resistant structures incorporated by the TOKI into the buildings, such as "raft foundation", a "tunnel formwork carrier system", and "high concrete strength", ensured that the buildings were not affected. The TOKI meticulously adhered to all applicable laws and regulations, particularly the Earthquake Regulation, while conducting project design studies. The analysis results revealed the locations of structural damage and allowed for the assessment of the structure's dynamic resistance. The authors of the report analyzed the recorded waveforms of surface vibrations to examine data about the ground motion at a regional scale and near-source ground motion. Two phenomena of similar intensity were selected for a detailed analysis to estimate the dynamic response of irregular structures subjected to earthquakes. This information is useful for studying the relationship between a long duration of motion and structural damage.

Author Contributions: Conceptualization, F.P. and T.T.; Methodology, F.P. and W.A.; Software, W.A.; Formal analysis, W.A.; Resources, T.T.; Writing—original draft, F.P.; Writing—review & editing, T.T. All authors have read and agreed to the published version of the manuscript.

Funding: This research received no external funding.

Institutional Review Board Statement: Not applicable.

Informed Consent Statement: Not applicable.

Data Availability Statement: The original contributions presented in the study are included in the article, further inquiries can be directed to the corresponding author.

Conflicts of Interest: The authors declare no conflicts of interest.

References

1. Menke, W.; Abend, H.; Bach, D.; Newman, K.; Levin, V. Review of the source characteristics of the Great Sumatra–Andaman Islands earthquake of 2004. *Surv. Geophys.* **2006**, *27*, 603–613. [CrossRef]
2. Papazachos, V.; Papazachou, K. *The Earthquakes of Greece*; Editions Ziti; University of Michigan: Ann Arbor, MI, USA, 1997.
3. Giacomelli, L.; Perrotta, A.; Scandone, R.; Scarpati, C. The eruption of Vesuvius of 79 AD and its impact on human environment in Pompeii. *Episodes* **2003**, *26*, 235–238. [CrossRef] [PubMed]
4. Satake, K.; Shimazaki, K.; Tsuji, Y.; Ueda, K. Time and size of a giant earthquake in Cascadia inferred from Japanese tsunami records of January 1700. *Nature* **1996**, *379*, 246–249. [CrossRef]

5. Rafferty, J.P. "New Madrid Earthquakes of 1811–1812". *Encyclopedia Britannica*. 9 December 2023. Available online: https://www.britannica.com/event/New-Madrid-earthquakes-of-1811-1812 (accessed on 12 January 2024).
6. Gutscher, M.-A. What Caused the Great Lisbon Earthquake? *Science* **2004**, *305*, 1247–1248. [CrossRef] [PubMed]
7. Wald, D.J.; Kanamori, H.; Helmberger, D.V.; Heaton, T.H. Source study of the 1906 San Francisco earthquake. *Bull. Seism. Soc. Am.* **1993**, *83*, 981–1019. [CrossRef]
8. Satake, K.; Atwater, B.F. Long-Term Perspectives on Giant Earthquakes and Tsunamis at Subduction Zones. *Annu. Rev. Earth Planet. Sci.* **2007**, *35*, 349–374. [CrossRef]
9. Plafker, G. *Tectonics of the March 27, 1964, Alaska Earthquake*; U.S. Geological Survey Professional Paper 543-I, 74 p. 2 sheets, scales 1:2,000,000 and 1:500,000; US Government Printing Office: Washington, DC, USA, 1969. Available online: https://pubs.usgs.gov/pp/0543i/ (accessed on 19 August 2024).
10. Kanaori, Y.; Kawakami, S.-I. The 1995 7.2 magnitude Kobe earthquake and the Arima-Takatsuki tectonic line: Implications of the seismic risk for central Japan. *Eng. Geol.* **1996**, *43*, 135–150. [CrossRef]
11. Norio, O.; Ye, T.; Kajitani, Y.; Shi, P.; Tatano, H. The 2011 eastern Japan great earthquake disaster: Overview and comments. *Int. J. Disaster Risk Sci.* **2011**, *2*, 34–42. [CrossRef]
12. Rafferty, J.P.; Pletcher, K. "Japan Earthquake and Tsunami of 2011". *Encyclopedia Britannica*. 10 January 2024. Available online: https://www.britannica.com/event/Japan-earthquake-and-tsunami-of-2011 (accessed on 12 January 2024).
13. Ichiyanagi, M.; Takai, N.; Shigefuji, M.; Bijukchhen, S.; Sasatani, T.; Rajaure, S.; Dhital, M.R.; Takahashi, H. Aftershock activity of the 2015 Gorkha, Nepal, earthquake determined using the Kathmandu strong motion seismographic array. *Earth Planets Space* **2016**, *68*, 1–6. [CrossRef]
14. Garini, E.; Gazetas, G. *The 2 Earthquakes of February 6th 2023 in Turkey—Preliminary Report*; NTUA: Athens, Greece, 2023.
15. *EN 1998-1:2004*; Eurocode 8 Design of structures for earthquake resistance—Part 1: General rules, seismic actions and rules for buildings. European Committee for Standardization: Brussels, Belgium, 2004.
16. *FEMA 356*; NEHRP Prestandard and Commentary for Seismic Rehabilitation of Buildings. American Society of Civil Engineering Reston, Virginia, Federal Emergency Management Agency: Washington, DC, USA, 2000.
17. *FEMA 440*; NEHRP Improvement of Nonlinear Static Seismic Analysis Procedures. Applied Technology Council (ATC-55 Project): Washington, DC, USA, 2005.
18. *ATC-40*; Seismic Evaluation and Retrofit of Concrete Buildings. Applied Technology Council: Redwood City, CA, USA, 1996; p. 94065.
19. Fajfar, P. *The Story of the N2 Method*; International Association for Earthquake Engineering (IAEE): Tokyo, Japan, 2021.
20. Zembaty, Z. Rockburst induced ground motion—A comparative study. *Soil Dyn. Earthq. Eng.* **2004**, *24*, 11–23. [CrossRef]
21. Habib, A.; Houri, A.A.; Habib, M.; Elzokra, A.; Yildirim, U. Structural Performance and Finite Element Modeling of Roller Compacted Concrete Dams: A Review. *Lat. Am. J. Solids Struct.* **2021**, *18*, e376. [CrossRef]
22. Habib, M.; Bashir, B.; Alsalman, A.; Bachir, H. Evaluating the accuracy and effectiveness of machine learning methods for rapidly determining the safety factor of road embankments. *Multidiscip. Model. Mater. Struct.* **2023**, *19*, 966–983. [CrossRef]
23. Pachla, F.; Kowalska-Koczwara, A.; Tatara, T.; Stypuła, K. The influence of vibration duration on the structure of irregular RC buildings. *Bull. Earthq. Eng.* **2019**, *17*, 3119–3138. [CrossRef]
24. Lavan, O.; De Stefano, M. *Seismic Behaviour and Design of Irregular and Complex Civil Structures*; Springer: Dordrecht, The Netherlands, 2014.
25. Zembaty, Z.; Stefano, M. *Seismic Behaviour and Design of Irregular and Complex Civil Structures II*; Springer: Dordrecht, The Netherlands, 2016.
26. Köber, D.; Stefano, M.; Zembaty, Z. *Seismic Behaviour and Design of Irregular and Complex Civil Structures III*; Springer: Dordrecht, The Netherlands, 2020.
27. Bento, R.; Stefano, M.; Köber, D.; Zembaty, Z. *Seismic Behaviour and Design of Irregular and Complex Civil Structures IV*; Springer: Dordrecht, The Netherlands, 2024.
28. Habib, A.; Yildirim, U. Distribution of strong input energy in base-isolated structures with complex nonlinearity: A parametric assessment. *Multidiscip. Model. Mater. Struct.* **2023**, *19*, 324–340. [CrossRef]
29. Habib, A.; Yildirim, U. Proposing unsupervised clustering-based earthquake records selection framework for computationally efficient nonlinear response history analysis of structures equipped with multi-stage friction pendulum bearings. *Soil Dyn. Earthq. Eng.* **2024**, *182*, 108732. [CrossRef]
30. Habib, A.; Alnaemi, A.; Habib, M. Developing a framework for integrating blockchain technology into earthquake risk mitigation and disaster management strategies of smart cities. *Smart Sustain. Built Environ.* **2024**. *ahead-of-print*. [CrossRef]
31. Habib, A.; Youssefi, I.; Kunt, M.M. Identification of pulse-like ground motions using artificial neural network. *Earthq. Eng. Eng. Vib.* **2022**, *21*, 899–912. [CrossRef]
32. Trifunac, M.D.; Brady, A.G. A study on the duration of strong earthquake ground motion. *Bull. Seismol. Soc. Am.* **1975**, *65*, 581–626.
33. Koehler, R. *Active Faults and Seismic Hazards in Alaska*; Alaska Division of Geological & Geophysical Surveys: Fairbanks, Alaska, 2018; p. 160. [CrossRef]
34. Wyss, M. A search for precursors to the Sitka, 1972, earthquake: Sea level, magnetic field, and P-residuals. *Pure Appl. Geophys.* **1975**, *113*, 297–309. [CrossRef]

35. Schell, M.M.; Ruff, L.J. Rupture of a seismic gap in southeastern Alaska: The 1972 Sitka earthquake (Ms 7.6). *Phys. Earth Planet. Inter.* **1989**, *54*, 241–257. [CrossRef]
36. Sykes, L.R. Aftershock zones of great earthquakes, seismicity gaps, and earthquake prediction for Alaska and the Aleutians. *J. Geophys. Res.* **1971**, *76*, 8021–8041. [CrossRef]
37. Tocher, D. The Alaska earthquake of July 10, 1958: Movement on the Fairweather fault and field investigation of southern epicentral region. *Bull. Seism. Soc. Am.* **1960**, *50*, 267–292. [CrossRef]
38. Ulrich, F.P. The Imperial Valley earthquakes of 1940*. *Bull. Seism. Soc. Am.* **1941**, *31*, 13–31. [CrossRef]
39. Trifunac, M.D.; Brune, J.N. Complexity of energy release during the Imperial Valley, California, earthquake of 1940. *Bull. Seismol. Soc. Am.* **1970**, *60*, 137–160.
40. Akinci, A.; Malagnini, L.; Sabetta, F. Characteristics of the strong ground motions from the 6 April 2009 L'Aquila earthquake, Italy. *Soil Dyn. Earthq. Eng.* **2010**, *30*, 320–335. [CrossRef]
41. Chioccarelli, E.; Iervolino, I. Near-source seismic demand and pulse-like records: A discussion for L'Aquila earthquake. *Earthq. Eng. Struct. Dyn.* **2010**, *39*, 1039–1062. [CrossRef]
42. DIANA. Finite Element Analysis User's Manual Release 10.2—Bing. [Online]. Available online: https://manuals.dianafea.com/d102/Analys/Analys.html (accessed on 19 May 2022).
43. Broyden, C.G. The Convergence of a Class of Double-rank Minimization Algorithms 1. General Considerations. *IMA J. Appl. Math.* **1970**, *6*, 76–90. [CrossRef]
44. Fletcher, R. *Practical Methods of Optimization*; Wiley: Hoboken, NJ, USA, 1988.
45. Fletcher, R. A new approach to variable metric algorithms. *Comput. J.* **1970**, *13*, 317–322. [CrossRef]
46. Goldfarb, D. A Family of Variable-Metric Methods Derived by Variational Means. *Math. Comput.* **1970**, *24*, 23–26. [CrossRef]
47. Shanno, D.F. Conditioning of Quasi-Newton Methods for Function Minimization. *Math. Comput.* **1970**, *24*, 647–656. [CrossRef]
48. De Domenico, D.; Gandelli, E.; Gioitta, A. Displacement-based design procedure for the seismic retrofit of existing buildings with self-centering dissipative braces. *Structures* **2024**, *62*, 106174. [CrossRef]
49. Yan, X.; Shu, G.; Rahgozar, N.; Alam, M.S. Seismic design and performance evaluation of hybrid braced frames having buckling-restrained braces and self-centering viscous energy-dissipative braces. *J. Constr. Steel Res.* **2024**, *213*, 108359. [CrossRef]

Disclaimer/Publisher's Note: The statements, opinions and data contained in all publications are solely those of the individual author(s) and contributor(s) and not of MDPI and/or the editor(s). MDPI and/or the editor(s) disclaim responsibility for any injury to people or property resulting from any ideas, methods, instructions or products referred to in the content.